



## PICOSECOND x-RAYS FROM SUBPICOSECOND-LASER-PRODUCED HOT-DENSE MATTER

D. UMSTADTER, J. WORKMAN, A. MAKSIMCHUK, X. LIU,  
U. ELLENBERGER, J. S. COE, and C.-Y. CHIEN

Center for Ultrafast Optical Science, University of Michigan, Ann Arbor, MI 48109-2099, U.S.A.

**Abstract**—Short-pulse, high-intensity laser-plasma interactions are investigated experimentally with temporally and spectrally resolved soft x-ray diagnostics. The emitted x-ray spectra from solid targets with various atomic numbers are characterized for a laser pulse width  $\tau_l \sim 400$  fs. With low contrast ( $10^5$ ), the x-ray spectrum in the  $\lambda = 40\text{--}100$  Å spectral region is dominated by line emission, and the x-ray pulse duration is found to be characteristic of a long-scale-length, low-density plasma. Bright, picosecond, broadband emission, characteristic of a short-scale-length, high-density plasma, is produced only when a high laser contrast ( $10^{10}$ ) is used. It is demonstrated experimentally that the pulse width of laser-produced x-ray radiation may be varied down to the picosecond time scale by adjusting the incident ultrashort-pulse laser flux. The results are found to be in qualitative agreement with the predictions of both a code-independent model of radiation from a collisionally dominated two-level ion and a hydrodynamics code coupled to a detailed-configuration atomic physics model. X-ray film measurements of conversion efficiency, along with pinhole camera measurements of the emission region, reveal very high x-ray brightness.

### I. INTRODUCTION

Short-pulse, high-intensity lasers interacting with solid targets make possible the study of a new class of laser-plasma interactions.<sup>1</sup> They are unique because, during the ultrashort laser pulse, relatively little expansion occurs, and the density scale length remains much less than the laser wavelength.<sup>2</sup> This makes possible the direct deposition of a significant amount of the laser energy at close to solid density. Steep plasma temperature and density gradients subsequently cause rapid cooling, resulting in highly non-equilibrium conditions and the concurrent emission of extremely bright ultrashort x-ray pulses. The latter may be used:

- (1) as a diagnostic of plasma conditions;
- (2) to study radiation hydrodynamics in a parameter regime that is otherwise inaccessible; and
- (3) for time-resolved diffraction, spectroscopy or microscopy studies of transient chemical, biological or physical phenomena.<sup>3</sup>

Factors controlling x-ray emission from ultrashort-laser-produced plasmas is a topic of considerable current interest. Harris and Kmetec<sup>4</sup> suggested theoretically the use of mixed species targets to increase the plasma cooling rate. Murnane et al<sup>5</sup> using a filtered x-ray streak camera—which provides high-temporal, but only poor spectral resolution—observed that the x-ray pulse width decreases with increasing laser contrast, indicating that only with high contrast can the laser energy be deposited at high plasma density. Sterns et al<sup>6</sup> used two laser pulses to control the plasma temperature, one to create a pre-plasma in order to increase the absorption of the other. Kieffer et al,<sup>7</sup> using high-spectral resolution, but time-integrated crystal spectroscopy in the keV region, implied the existence of a solid-density plasma from x-ray linewidths. Prior to those presented here, the only results of simultaneous high-temporal and high-spectral resolution measurements were from experiments with relatively long laser pulses ( $\tau \geq 10$  ps) (see for example Riley et al<sup>8</sup>). In this case, the laser interacts primarily with its critical density as the plasma expands

during the laser pulse. Murnane et al<sup>9</sup> suggested the use of structured targets to increase laser energy absorption. Umstadter et al<sup>10</sup> and, later, Milchberg et al<sup>11</sup> discussed theoretically the temperature dependence of recombination continuum radiation.

In the most general terms, the duration of x-ray line emission from a plasma ion is determined primarily by the dynamics of its lifetime and electron energy-level populations. At high plasma density, these factors depend on the rate of collisions between electrons and ions, which, in turn, depends on the collision cross section, and thus the relative strength of the plasma electron's kinetic energy with respect to the ion's Coulomb field. This varies both with the peak value and with the change in the electron temperature. It turns out that the change in electron temperature (heating or cooling rate) is relatively independent of the peak value of the electron temperature. The peak electron temperature can be increased or decreased by changing just one parameter, the laser energy flux density, or, if the laser pulse width is kept constant, the laser intensity. In this paper, we demonstrate experimentally, and explain theoretically, the details of how the pulse duration of soft x-ray lines emitted from high-temperature and high-density plasmas can be controlled by controlling the incident laser intensity, and thus the peak electron temperature. Specifically, we show that a lower peak electron temperature leads to a shorter pulse of x-rays, and that this pulse can be reduced in duration to the picosecond time scale.

In order to make these measurements, we employ high-temporal and spectral resolution x-ray spectroscopy in conjunction with intense high-contrast subpicosecond laser pulses. The former is made possible by the use of a grazing-incidence grating-spectrometer, facilitating high-resolution spectroscopy in the soft x-ray photon-energy range. Soft x-ray photons in this energy range (40–300 eV) correspond to the peak emission of a blackbody with an average temperature equal to that typically reached by these ultrashort-laser-produced plasmas ( $T_e < 1$  keV),<sup>7,12,13</sup> and can thus originate from ion stages that are equal to, or well below, the highest. However, for the same reason, harder x-rays, in the multi-keV photon-energy range, which are usually measured by use of crystal spectroscopy, have a lower photon flux, and only originate from the highest ionization stages. Moreover, the relatively higher flux of these softer x-rays permits simultaneous temporal and spectral resolution over a larger range of laser intensities ( $10^{15} \leq I \leq 10^{17}$  W/cm<sup>2</sup>) and, thus, over a larger range of peak electron temperatures.

In Sec. II, we present a general theoretical discussion of the factors controlling the pulse width of the x-ray emission. Our experimental results are well explained, at least qualitatively, with a simple code-independent model of radiation from a collisionally dominated two-level ionic system. In Sec. III, we discuss the results of our detailed numerical model. Comparison with the predictions of this more detailed numerical model of a radiating plasma—including a hydrodynamics code, coupled to a detailed-configuration atomic physics model—indicates that significant amounts of emission come from non local thermodynamic equilibrium (non-LTE) regions and that opacity effects are important. The experimental arrangement is discussed in Sec. IV and experimental results in Sec. V. In Sec. VI, the results of our numerical simulation with our experimental data are compared and discussed. Finally in Sec. VII, we present a summary.

## II. THEORY

Theory can provide some general predictions about how the plasma parameters and the x-ray emission should evolve. Of course, a plasma can generate x-ray line emission of given photon energy  $h\nu$  only if it reaches an ionization stage corresponding to that transition. This happens when the electron temperature,  $T_e$ , reaches the “ionization temperature” for that stage, which in equilibrium is taken to be a fraction of (approximately one third) the corresponding ionization potential. In the absence of radiative heating, a given region of the plasma is heated either by direct deposition of laser energy or by diffusion of heat from neighboring regions. The rise time of the x-ray pulse is roughly determined by the heating time.

The plasma cools both by expansion into the vacuum and by heat conduction into the colder regions of the solid. The decay of the x-ray emission will be controlled by these cooling processes. The bound emission from any local region of the plasma, at any given time, is determined by the population densities of the various allowed energy levels. More precisely, the emission will be

determined by the source function, which is the emissivity divided by the opacity,  $\epsilon/\kappa$ . For bound-bound emission the source function is given by:

$$S = \frac{n_u A_{ul} (h\nu_{ul}/4\pi) \phi(\nu)}{n_l [1 - (n_u g_l/n_l g_u)] f_{ul} \phi(\nu)}, \quad (1)$$

where  $n_u$  and  $n_l$  are the upper and lower state densities of the transition considered and  $g_u$  and  $g_l$  are the degeneracies of the upper and lower states.  $A_{ul}$  is the spontaneous emission rate,  $f_{ul}$  is the oscillator strength,  $h\nu_{ul}$  is the energy of the transition and  $\phi(\nu)$  is the line broadening function. Since most of these factors are constants in time, we see that the temporal dependence of the emission is given by:

$$S \propto \frac{n_u/n_l}{1 - (n_u g_l/n_l g_u)}. \quad (2)$$

In general  $g_l/g_u$  will be less than one. This gives  $S$  an almost linear dependence on  $n_u/n_l$ . (As  $n_u/n_l$  approaches one the dependence is only slightly non linear since  $g_l/g_u$  will be less than one.) Therefore, the time history of the emission is determined by the time history of the upper and lower state density ratio. It is, therefore, necessary to consider the factors controlling this ratio.

In a high-density plasma, collision rates play the largest role in determining the population densities, as long as the collisional excitation and de-excitation rates are not less than the spontaneous decay rate,  $A_{ul}$ . Because of the high densities and relatively low temperatures produced in these plasmas, we will neglect contributions of rates containing radiation fields, as they are generally much less than the collision rates. If we consider a two-level system, consisting of  $n_u$  and  $n_l$ , the populations are directly coupled. For the conditions of our experiment, lithium-like ions at high density (which gives rise to continuum lowering), a two-level system is not unreasonable. A decrease in  $n_u$  means an increase in  $n_l$ , and a decrease in the ratio  $n_u/n_l$ . We can consider two collision rates. One rate excites an electron from  $n_l$  to  $n_u$ , and the other rate de-excites an electron in  $n_u$  down to  $n_l$ . In general we expect that a more highly excited ion, of the same species and ion state, will present a larger cross section for electron collisions; the excited electron is further from the nucleus and, therefore, has a lower potential for screening the Coulomb field. This leads us to expect that the collisional excitational rate will be less than the collisional de-excitation rate. This expectation is borne out by the numerous detailed derivations and experimental measurements of collisional cross sections.<sup>14</sup> When these cross sections are integrated over Maxwellian velocity distributions for the electrons, we obtain the dependence on temperature and density, found in the collisional excitation and de-excitation rates. The de-excitation rate per ion is proportional to  $n_e/\sqrt{T_e}$ , and the excitation rate per ion is proportional to  $n_e \exp(-h\nu_{ul}/kT_e)/\sqrt{T_e}$ .<sup>14-16</sup> As expected, we see that the higher the electron temperature, the smaller the difference between the two rates and, therefore, the smaller the change in the ratio  $n_u/n_l$ . In other words, the difference in the Coulomb field between these two excited states becomes less distinguishable by the electron as its kinetic energy increases. As the electron temperature decreases towards the energy difference of the two excited states, the difference between the rates begins to change more rapidly with changing temperature. To relate this back to the emission, we see that the population ratio,  $n_u/n_l$ , and therefore the emission, changes slowly with changes in electron temperature at high electron temperatures ( $T_e \gg h\nu_{ul}$ ). As the electron temperature approaches the transition energy, small changes in temperature translate into large changes in emission. A higher peak temperature would mean a slower decrease in emission for a given cooling rate and, therefore, a longer pulse duration. Experimentally, this means that we expect to see longer x-ray pulses with long tails at high laser intensity, and shorter x-ray pulses at low laser intensities.

The above argument is quite general for high-density plasmas, and can be extended to the inclusion of excitation and de-excitation rates, which are electron temperature independent. When the de-excitation rate corresponding to spontaneous emission,  $A_{ul}$ , is included, a similar dependence of pulse duration on electron temperature is expected, as long as the collision rates are not smaller than the spontaneous rate. Obviously, if the collision rates are much lower than the spontaneous

rates, there will be very little dependence of pulse duration on electron temperature, since  $A_{ul}$  is independent of electron-temperature. The collision rates tend to approach the spontaneous rate as the density drops. By the time the density has dropped significantly, the temperature has also dropped. This means that the collisional de-excitation rate has become much larger than the excitation rate. Therefore the spontaneous rate will merely have the effect of steepening the slope of the emission decay.

In very-high-density regions of the plasma, where the collision rates are much larger than any other rates, the recombination rate will determine the pulse duration. We will see, however, that the pulse duration still has the same dependence on temperature. In an LTE region of the plasma, the ionization stage would closely follow changes in  $T_e$  according to the Saha equation. Significant emission from a particular ionization stage will occur only when the plasma is predominantly in that ionization stage. In the LTE case, the maximum average ionization state  $\bar{Z}_{\max}$  would be determined by the maximum plasma temperature. As the temperature drops, the average ionization stage will drop below some threshold ionization stage for bound-bound emission from a particular ion species ( $\bar{Z}_0$ ). If  $\bar{Z}_{\max} \gg \bar{Z}_0$  then it will take some time ( $\tau_0$ ) to drop below this threshold. The rate at which  $\bar{Z}_0$  drops with temperature is again determined by the factor  $\exp(-hv/kT_e)$ . At low  $T_e$ , where  $kT_e \ll hv$ ,  $\bar{Z}_0$  will drop very rapidly. As  $T_e$  approaches  $hv$ , the change in  $\bar{Z}_0$  will become more gradual. For very large  $T_e$  there is very little change in  $\bar{Z}_0$ . The longer  $T_e$  stays above  $hv$ , the longer  $\tau_0$  will be, and the more gradual the slope of emission decay.

Even though the three-body recombination rate drops as the density drops, with the square of the electron density, the emission can still have a very strong collisional dependence through the collisional excitation and de-excitation rates, which depend linearly on the electron density. In these somewhat-lower-density, non-LTE regions, the ionization stage becomes decoupled from the temperature, and the ionization stage will stay relatively constant on the time scale of tens of picoseconds. These assumptions were implicit in the above discussion in which only collisional excitation and de-excitation were considered.

It may thus be concluded from the arguments presented above that in either case, LTE or non-LTE, in order to obtain short-duration x-ray pulses, the re-emission peak electron temperature must not much exceed a certain minimum value. However, if the temperature is kept too low, the x-ray intensity will be greatly reduced.<sup>17</sup> This means that there exists an optimal maximum electron temperature, and thus an optimal laser intensity, for a given target element to obtain short, bright x-ray pulses. In order to maximize the total x-ray flux, the total number of x-ray emitters should also be maximized. This can be done by maximizing both the plasma density and the radial dimensions of the region over which the optimal temperature conditions exist. The former means that the shortest laser pulse should be used, in order to increase the direct deposition of laser energy at solid density. The latter implies that the laser spot size should be maximized but, of course, in such a way that the peak laser intensity will be equal to its optimal value for the laser energy available.

The above description of pulse duration and electron temperature only involves plasma conditions locally, where the x-rays originated. However, due to finite plasma size, a detector external to the plasma will integrate the contributions from each local region along the radiation propagation path. Thus, absorption, re-emission, escape, stimulated emission and Doppler shifts must also be considered, which—by coupling the radiation from separate regions—makes the problem a global one. For instance the x-ray opacity of the under-dense plasma regions can act to reduce the observed pulse width and flux of the x-ray emission that originated from the more dense regions. On the other hand, radiation trapping—due to the multiple absorptions and re-emissions, which can occur as the radiation traverses the high-opacity region—may act to stretch the observed x-ray pulse width. The temporal and spectral characteristics of the observed x-ray emission are determined by the complex interplay between these global effects and local plasma conditions. Since these effects are both time- and space-dependent, the complexity of the problem obviously necessitates detailed numerical analysis.

Although we studied both gold and aluminum experimentally, only the latter was investigated numerically, as discussed in Sec. III. This is because its lower density of lines makes the calculation of its emission less computationally expensive, and its emission lines more distinguishable experimentally.

### III. NUMERICAL ANALYSIS

The concepts discussed in Sec. II are illustrated by the results of a numerical analysis of the interaction. Our one-dimensional hydrodynamics code solves the conservation equations of energy, momentum, and mass for a two-fluid plasma. The fluid equations are coupled self-consistently to the Helmholtz equation of the laser field for energy and momentum deposition in the plasma.<sup>18</sup> An average-atom non-LTE model<sup>19</sup> is used to determine the ionization balance as a function of temperature and density. Thermal conductivity is determined by the Spitzer formula with tabulated corrections for low temperatures,<sup>20</sup> and a flux limiter set to one-tenth the free-streaming velocity. The output of the hydrodynamics code, plasma density, and temperature of each cell is then used as input to a detailed-configuration, time-dependent, atomic-physics package, FLY,<sup>21</sup> to calculate the population densities and ultimately the spectral emission. Included in the atomic physics package are the effects of the Stark broadening and local opacity. A Planckian radiation field is used to determine photo-excitation and stimulated emission rates. The integrated emission along  $z$  is determined by transporting the emission from each cell through the plasma while incorporating the effects of the opacity and motional Doppler shifts. Global effects of opacity are determined by the simple equation,  $I_{n+1} = I_n(1 - \exp(\kappa L))$ , where  $I_{n+1}$  is the total emission after traversing cell  $n + 1$  and  $I_n$  is the total emission after traversing the previous cell.  $\kappa$  is the frequency-dependent opacity of cell  $n + 1$  and  $L$  is the length of cell  $n + 1$ .

Results of the numerical analysis predict a pulse duration of 2.2 ps for the Al $\text{X}\text{I}$   $2p-3d$  doublet at  $\lambda = 52.4 \text{ \AA}$  at a laser intensity of  $5 \times 10^{17} \text{ W/cm}^2$ , and a pulse duration of 1.9 ps at a laser intensity of  $5 \times 10^{16} \text{ W/cm}^2$ . The peak electron temperature was found to be about 1 keV for the highest intensity case and about 400 eV for the  $5 \times 10^{16} \text{ W/cm}^2$  case. As expected, the predicted pulse duration becomes shorter as the laser intensity is decreased in the simulation.

The effects of Doppler shifts on the line transport were found to be extremely small, due to Stark broadening at high density. Opacity played a very large role in the line transport, reducing the pulse duration from 20 ps to 2 ps at  $I = 10^{17} \text{ W/cm}^2$ . (Relative pulse durations for the different laser intensities were also greatly reduced by the inclusion of optical depth effects, as can be seen in Fig. 7.) Pulse lengthening, due to radiation trapping, was estimated,<sup>22</sup> but found to have relatively little effect as collision rates were larger than the spontaneous rate of 1 ps for this transition (Al $\text{X}\text{I}$   $2p-3d$ ), in almost all regions of the plasma. Simulations were also carried out for the Al $\text{X}\text{I}$   $2s-3p$  resonance transition. Having obtained very similar results, we will not discuss this transition, and will concentrate instead on the Al $\text{X}\text{I}$  transition, already discussed.

### IV. EXPERIMENTAL ARRANGEMENT

In performing the experiment, we used a 400-fs terawatt Nd:glass laser system based on chirped pulse amplification, with a contrast ratio of the fundamental 1.06- $\mu\text{m}$  laser light measured to be  $5 \times 10^5$ , which was increased to  $10^{10}$  by frequency doubling. An off-axis parabolic mirror is used to focus the  $S$ -polarized  $2\omega$ -laser radiation on a solid target at normal incidence to a minimum spot size of  $15 \mu\text{m}$ , corresponding to a maximum intensity in the second harmonic light of  $5 \times 10^{17} \text{ W/cm}^2$ . Targets included 4- $\mu\text{m}$  thick aluminum and gold deposited onto silicon wafers. In order to decrease the incident flux on the target, the laser spot size was defocused while keeping the total laser energy constant. The soft x-ray emission is spectrally dispersed using an imaging flat-field grazing-incidence variable-spaced grating spectrometer located at  $40^\circ$  to the target normal. With a slit width of  $200 \mu\text{m}$  we obtain a spectral resolution,  $\delta\lambda/\lambda$ , of about 200 at  $50 \text{ \AA}$ . Time-resolved spectra are obtained in a single shot, using an x-ray streak camera with a potassium bromide photo-cathode supported by a Lexan film, coupled to the spectrometer. The temporal resolution is 5 ps. Temporally and spectrally dispersed images are read out to a computer with a CCD camera. A 20- $\mu\text{m}$  x-ray pinhole camera is filtered with  $25 \mu\text{m}$  of Be and  $6000 \text{ \AA}$  of Al, and coupled to an intensified micro-channel plate detector to monitor the laser spot size and emission region. Two PIN diodes filtered with  $50 \mu\text{m}$  and  $100 \mu\text{m}$  of Be were used to monitor relative keV x-ray emission levels and to monitor the reproducibility of each interaction. A calibrated calorimeter was used to monitor laser energy on each shot. To obtain quantitative conversion

efficiencies of the laser radiation into x rays, in the range 1.5–5-keV, DEF film was used with steps of Be filters of different thicknesses and with known characteristic absorption curves.<sup>24</sup>

## V. EXPERIMENTAL RESULTS AND DISCUSSION

Figures 1(a) and (b) show the temporally and spectrally dispersed emission from a laser-irradiated aluminum target ( $Z = 13$ ) for two different laser contrasts with the same laser intensities, showing the x-ray amplitude (grey scale in units of CCD counts) vs wave-length (vertical axis in units of Å) and time (horizontal axis in units of picoseconds). Figure 1(b) is the emission using 1.06- $\mu\text{m}$  light to irradiate the target. One sees that the emission is dominated by lines and that the pulse duration is long,  $\tau \sim 50$  ps (FWHM). Figure 1(a) shows the emission using  $2\omega$  (0.53- $\mu\text{m}$ ) irradiation, corresponding to high-contrast illumination of the target. Figures 1(c) and (d) are line-outs in wavelength at the time of peak emission in the two contrast cases. Note that in the high-contrast case the emission is fairly continuous over the entire wavelength range, characteristic of high-density spectral broadening, and that the pulse duration [ $\tau \sim 15$  ps (FWHM)] is shorter than in the low-contrast case. In both figures, the sharp cutoff near the C K-edge (44 Å) is due to absorption by the Lexan film that supports the potassium bromide photo-cathode. Figure 1 clearly shows the importance of laser contrast in obtaining a high-density plasma, and consequently shorter bursts of x-ray emission.

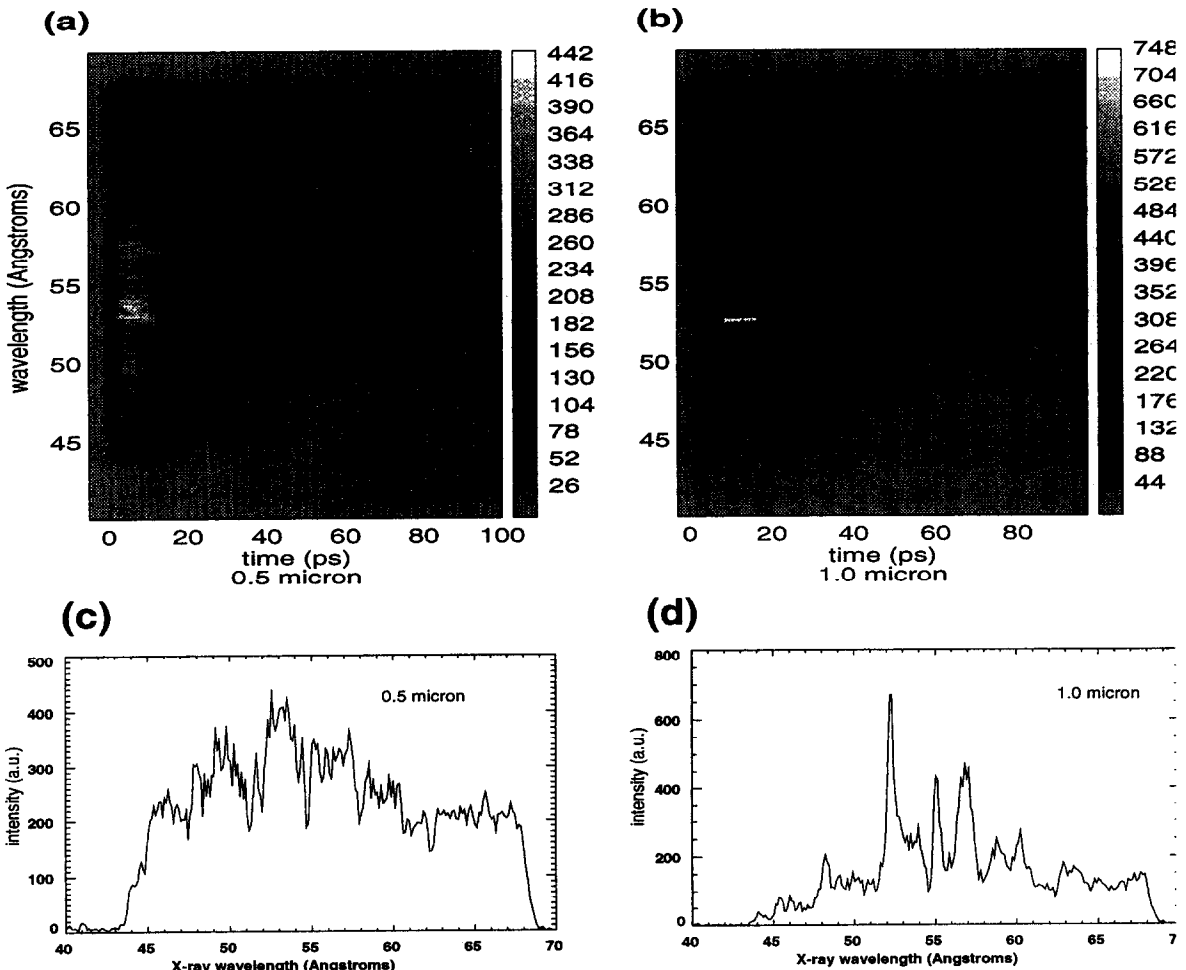


Fig. 1. Streaked aluminum x-ray spectra obtained in a single shot with a high-resolution grazing incidence spectrometer: (a) and (c) using  $2\omega$  laser irradiation, corresponding to high-contrast conditions; (b) and (d) using  $1\omega$  laser irradiation, corresponding to low-contrast conditions. Spectral line-outs (c) and (d) are taken at the peak of the emission.

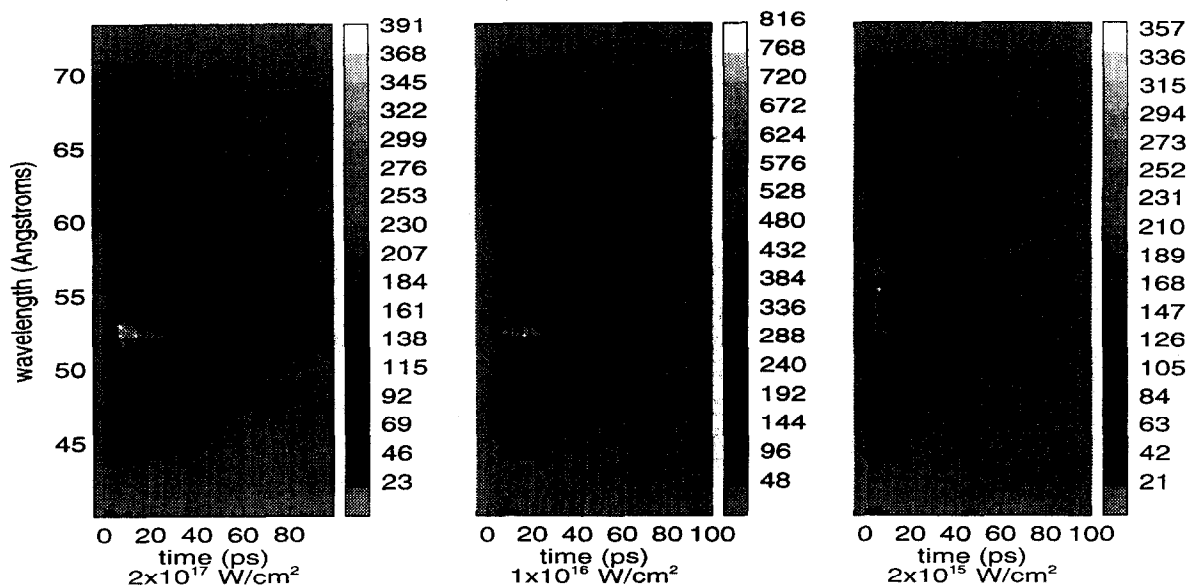


Fig. 2. Temporally and spectrally resolved aluminum x-ray emission obtained from three different laser intensities.

Figure 2 illustrates the arguments presented in Sec. II by showing single-shot aluminum x-ray emission using high-contrast conditions for three different laser intensities, ranging from  $2.0 \times 10^{17}$  down to  $2.0 \times 10^{15} \text{ W/cm}^2$ . The obvious trend, as predicted, is that the x-ray pulse duration decreases as the laser intensity is decreased. High-density effects are quite obvious in all cases, as the initial Stark-broadened emission is virtually continuous over the entire wavelength region shown. One can see the discrete line emission appear as the density has dropped in time. Note that the signal level has not decreased with laser intensity as we have kept the collected x-rays relatively constant by enlarging the focal spot of the laser. This eliminates any effect of dynamic range in the system as a factor in changing the measured relative pulse durations.

Figure 3 shows a comparison of amplitude-normalized temporal profiles from the above plots of the Al $1s^2p-1s^23d$  line ( $\lambda = 52.4 \text{ \AA}$ ) obtained for  $2\omega$ -irradiation for a range of laser flux densities. Note the pronounced decrease of the x-ray pulse width as the laser intensity is decreased. In the low-intensity case, the FWHM of the x-ray pulse approaches the streak camera limit. The rise time is short in all cases as expected from the rapid heating. (The starting positions of the plots relative

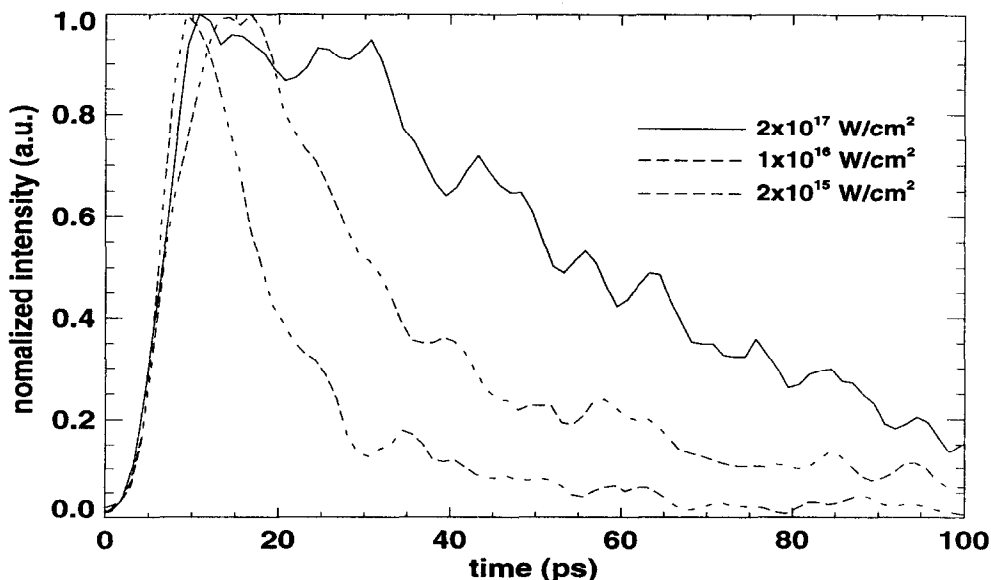


Fig. 3. Comparison of amplitude-normalized temporal profiles of the Al $1s^2p-1s^23d$  transition obtained experimentally, showing the reduction of the pulse duration with decreasing laser intensity.

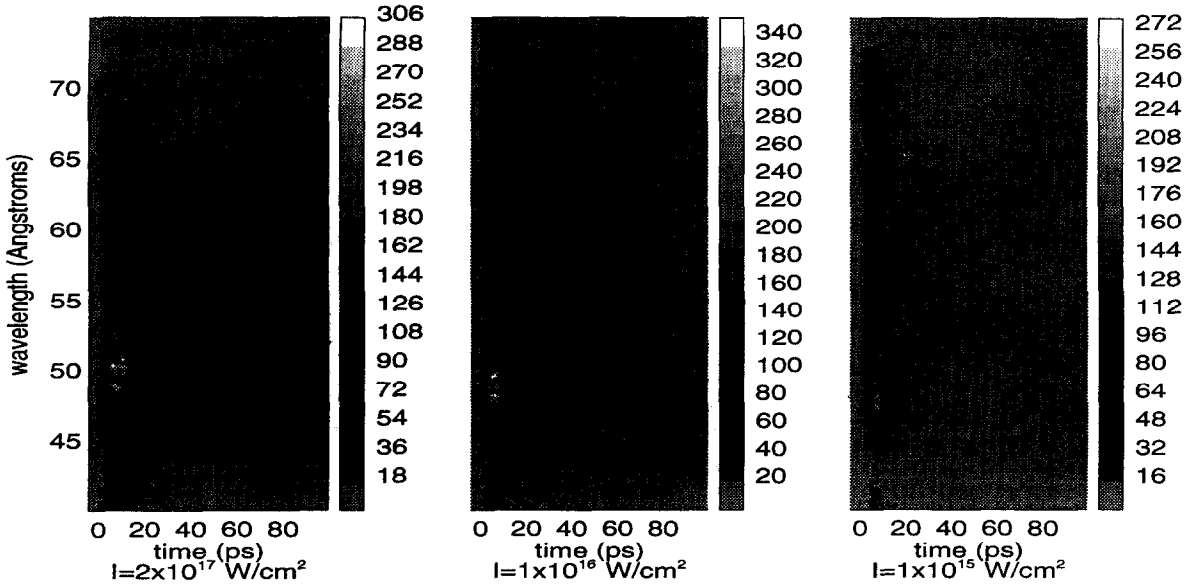


Fig. 4. Experimentally measured streaked gold spectra.

to the laser pulse and each other are unknown.) The fall time is observed to be shorter and the slope of the decay much steeper in the lowest-laser-intensity case, as expected from the arguments in Sec. II.

The results of the gold emission in this wavelength region are shown in Fig. 4. We can see shorter pulse durations, with decreasing laser intensity, than in the case with aluminum. This is presumably due to the higher electron densities, that one would expect in a high *Z* material such as gold, which lead to higher collision rates. The emission from the gold is extremely continuous even at late times, due to the high density of emission lines.

Figure 5(a) shows the comparison of measured x-ray pulse duration as a function of laser flux for two different materials, aluminum and gold. The averaged experimental aluminum pulse widths at  $\lambda = 52.4 \text{ \AA}$  are shown as crosses. The gold data, also at  $\lambda = 52.4 \text{ \AA}$  is represented by the open diamonds. Data was averaged over 3 to 5 laser shots with the standard deviation of the pulse duration shown by the vertical error bars. Horizontal error bars indicate spot size uncertainty. The lower value is the measured spot size through Be filters on a pinhole camera with a resolution of

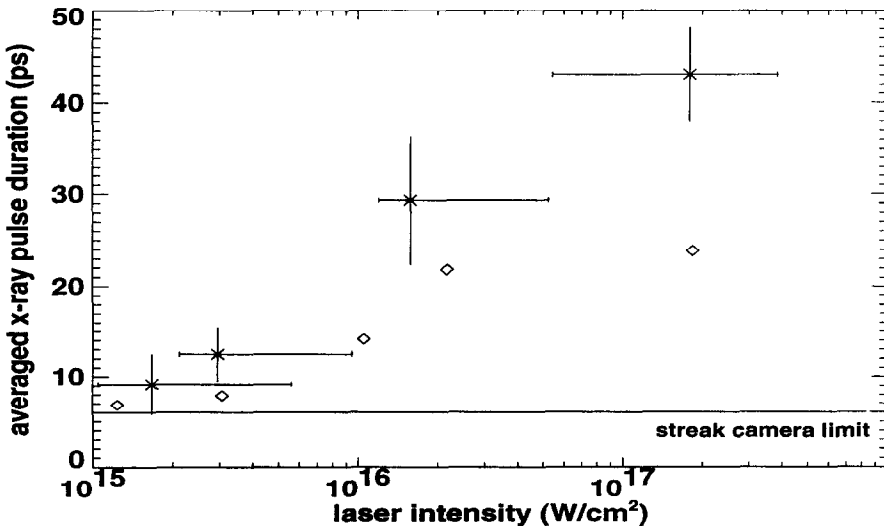


Fig. 5. Duration of the x-ray emission, at ( $\lambda = 52.4 \text{ \AA}$ ), vs laser intensity as measured experimentally: Al( $1s^2sp-1s^23d$ ) ( $\times$ ) and Au ( $\diamond$ ).

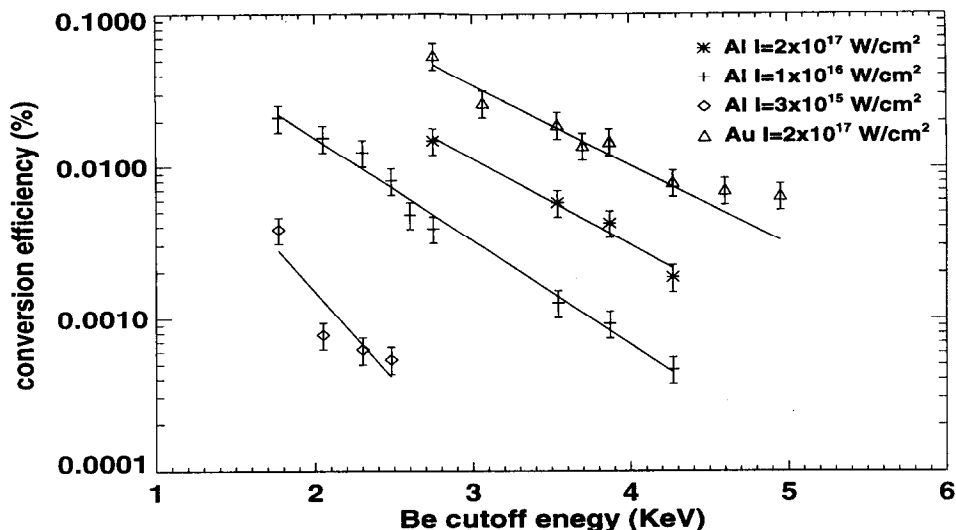


Fig. 6. Measured x-ray conversion efficiency for aluminum and gold solid targets for a range of laser fluxes.

20  $\mu\text{m}$ . The higher intensity value was determined from optical measurements of the spot-size at low laser energy ( $< 0.5$  mJ). For the same laser intensity, the gold x-ray pulse duration was found to be as little as half the aluminum pulse duration and was streak-camera-limited at the lowest intensity.

Data on conversion efficiency of laser radiation into x-rays in the range 1.5–5 keV are shown in Fig. 6. Note that conversion efficiency for the gold target is about four times higher than for the aluminum target due to the higher density of emission lines in this spectral region. For the highest laser fluxes on target the conversion efficiency can reach about 0.1% (up to a mJ) for the x-ray photons with  $h\nu \geq 1$  keV. The conversion efficiency is increasing toward longer wavelength implying even higher conversion efficiency, and therefore even higher brightness, in the soft x-ray region discussed above.

## VI. DISCUSSION

To illustrate the concepts put forth in Sec. II we will discuss the details of the numerical simulation and compare these to the experimental data. Because the integrated output of the numerical simulation is very sensitive to the radiation transport model used, it will be more useful to look at the integrated source function without the effects of radiation transport.

By summing the emission along the  $z$ -axis without including the global contribution of opacity, we can obtain some insight into the total contributions of the model discussed in Sec. II. The effects of radiation trapping and Doppler shifts were found to be small and are, therefore, not included. However, because radiation trapping is small, we know that the collision rates, in our simulation, must have been larger than spontaneous rates in most regions of the plasma. Figure 7 shows the simulated, integrated, normalized emission, without opacity, as a function of time for three different laser intensities. The emission is averaged over a spectral range of 52.2–52.5  $\text{\AA}$  corresponding to the resolution of the spectrometer used in the experiment. As mentioned earlier, the peak temperatures reached from 1 keV (for the highest intensity) to a few hundred eV (for lower laser intensities). The electron-temperature time profiles are very similar in the different laser-intensity cases, with differences only in the absolute electron temperature values. The electron temperature drops rapidly from its peak value to a few tens of eV in a few picoseconds in all regions of the plasma. We therefore see that the LTE region of the plasma is not the only contributor to the tens-of-picoseconds pulse durations. We can then conclude that the lower-density, non-LTE regions are very significant in determining the pulse duration. As predicted in Sec. II, we see in Fig. 7 that the tail of the pulse has a more gradual slope at higher laser intensity and becomes steeper as the laser intensity is decreased. The longer x ray pulses correspond to higher average electron temperatures as expected. As we have seen in Fig. 3, there is a similar trend in the

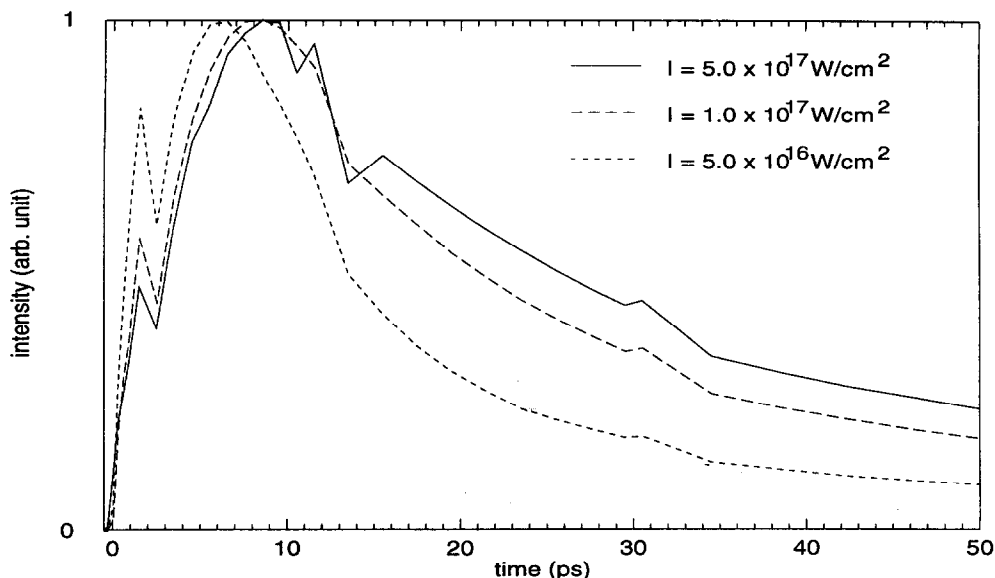


Fig. 7. Comparison of amplitude-normalized spatially integrated temporal profiles of the  $\text{AlK}\alpha$   $1s^2 2p-1s^2 3d$  emission obtained numerically. Note: emission is the integrated source function of each cell.

experimentally measured pulse tail. We can infer from Fig. 6 that the average experimental electron temperatures also increased with higher laser intensities. Higher x-ray yields, in the keV region, with increasing laser intensity, imply higher electron temperatures. The x-ray yield increased with higher laser intensity, despite the fact that the emission region was reduced by decreasing the laser spot size. We can, therefore, claim to have qualitative similarities between experiment and simulation, which both agree with the simple model presented.

These qualitative similarities between the experimental pulses and the simulated pulses without global opacity become more subtle when our radiation transport model (which includes opacity) is included in our calculations. Several obvious reasons for discrepancy between simulation and experiment can be suggested. Our simple model for opacity may be quite inadequate to describe the radiation transport in this highly non equilibrium, high-density plasma. Large magnetic fields<sup>23</sup> might also influence the dynamics of the plasma, and therefore the emission. The effects of magnetic fields would be extremely difficult to include in a one-dimensional simulation. Current laser absorption, equation-of-state and thermal conductivity models may also be inaccurate for these types of plasmas. Contributions from detailed Be-like satellite emission, which might have some contribution in the red wings of the Li-like transition that we have considered, are not included in our atomic physics package. Regardless of the current lack of a comprehensive model for emission from these unique plasmas, our results are explained by the fact that the pulse duration, as a function of laser intensity, is controlled by the temperature dependence in the collision rates; and therefore, at higher laser intensity, the average temperature will be higher and the pulse will be longer.

## VII. SUMMARY

To summarize, we have shown that the pulse width of soft x-rays emitted from these high-density plasmas is controlled by the temperature dependence of the collision rates. Consequently, the pulse duration may be reduced—without sacrificing the total amount of emitted photons—by adjusting the laser focal spot size, and thereby the incident laser intensity. These experimental results are found to agree with a simple code-independent model, and to be in qualitative agreement with the predictions of our hydrodynamics code coupled to an atomic physics model. The conversion efficiency of the high-contrast subpicosecond laser pulses into ultrashort soft x-ray pulses can be as high as a few tenths of a percent. The emission from gold targets in the x-ray region of  $50 \text{ \AA}$  was observed to be an-order-of-magnitude brighter than the emission from the aluminum, due both to its shorter pulse duration and higher x-ray yield.

*Acknowledgements*—This work was partially funded by the National Science Foundation Center for Ultrafast Optical Science, Contract No. PHY8920108 and the University of California Los Alamos National Laboratory GB/020165/AL/03. The authors would like to thank G. Mourou, R. Lee and J. Apruzese for useful discussions and encouragement.

## REFERENCES

1. G. Mourou and D. Umstadter, *Phys. Fluids B* **4**, 2315 (1992).
2. M. M. Murnane, H. C. Kapteyn and R. W. Falcone, *Short Wavelength Coherent Radiation: Generation and Application*, R. W. Falcone and J. Kirz, eds. Vol. 2, p. 189, Optical Society of America, Washington, DC (1989).
3. *OSA Proceedings on Short Wavelength Coherent Radiation: Generation and Applications, 1991*, P. Bucksbaum and N. Ceglio, eds., p. 11, Optical Society of America, Washington, DC (1991).
4. S. E. Harris and J. D. Kmetec, *Phys. Rev. Lett.* **61**, 62 (1988).
5. M. M. Murnane et al, *Phys. Rev. Lett.* **62**, 155 (1989).
6. D. G. Stearns, O. L. Landen, E. M. Campbell, and J. H. Scofield, *Phys. Rev. A* **37**, 1684 (1988).
7. J. C. Kieffer et al, *Bull. Am. Phys. Soc.* **37**, 1468 (1992).
8. D. Riley et al, *Phys. Rev. Lett.* **69**, 3739 (1992).
9. M. M. Murnane, H. C. Kapteyn, S. P. Gordon, J. Bokor, E. N. Glytsis, and R. W. Falcone, *Appl. Phys. Lett.* **62**, 1068 (1993).
10. D. Umstadter et al, *Bull. Am. Phys. Soc.* **34**, 1364 (1989).
11. H. Milchberg et al, *Phys. Rev. Lett.* **67**, 2654 (1991).
12. R. C. Mancini, *J. Phys. B: At. Mol. Opt. Phys.* **27**, 1671 (1994).
13. R. P. Town, A. R. Bell and S. J. Rose, *Phys. Rev. E* **50**, 1413 (1994).
14. D. M. Cochrane and R. W. P. McWhirter, *Phys. Scripta* **28**, 25 (1983).
15. R. Mewe, *Astron. Astrophys.* **20**, 215 (1972).
16. H. Van Regemorter, *Astrophys. J.* **136**, 906 (1962).
17. R. Eisberg and R. Resnick, *Quantum Physics of Atoms, Molecules, Solids, Nuclei and Particles*, Wiley, New York (1985).
18. X. Liu, Thesis, University of Michigan (1994).
19. S. J. Rose, *JQSRT* **36**, 389 (1986).
20. L. Spitzer, *Physics of Fully Ionized Gases*, Interscience, New York (1962).
21. R. W. Lee et al, *JQSRT* **32**, 91 (1984).
22. J. P. Apruzese, *Phys. Rev. E* **47**, 2798 (1993).
23. R. N. Sudan, *Phys. Rev. Lett.* **70**, 3075 (1993).
24. B. L. Henke et al, *J. Opt. Soc. Am. B* **3**, 1540 (1986).